Measurement of Length and Position with Frequency Combs

Measurement of Length and Position with Frequency Combs

C Weimann[1,2*], F Hoeller[3], Y Schleitzer[3], C A Diez[3], B Spruck[3], W Freude[1,2], G Boeck[4], C Koos[1,2*]

[1]Institute of Photonics and Quantum Electronics, Karlsruhe Institute of Technology (KIT), Karlsruhe, Germany
[2]Institute of Microstructure Technology, KIT, Karlsruhe, Germany
[3]Corporate Research and Technology, Carl Zeiss AG, Oberkochen, Germany
[4]Microwave Engineering Lab., Berlin Institute of Technology, Berlin, Germany

*Email: claudius.weimann@kit.edu, christian.koos@kit.edu

Abstract. We show two different absolute distance measurement methods with micrometer accuracy based on frequency combs, and we discuss possible applications. Using a mode-locked laser and MEMS-based tracking optics, we measure the 3D position of a retroreflector within 10 ms and with a 24 µm volumetric accuracy. We also investigate modulator-based combs and show that they enable highly sensitive surface topography measurements with microsecond acquisition times and micrometer precision. Moreover, the potential for photonic integration of frequency comb sources is explored.

1. Introduction

Dimensional metrology such as measurement of distance and position in three-dimensional (3D) space are of great importance in many scientific fields as well as in industrial applications such as inline inspection, robotics and machinery assembly. Optical 3D position measurement systems can be used for large-scale or inline measurements, ideally in combination with an optical sensor head to enable non-contact, fast and precise investigation of object surfaces. In this paper, we will present the use of optical frequency combs to fulfil these measurement tasks, first discussing the optical measurement of 3D coordinates and then the realization of an optical surface sensor.

Different approaches for an optical position measurement have been taken in the past, such as laser trackers [1, 2], photogrammetry [3, 4], camera or diode-based triangulation [3, 5, 6] and multilateration [7–11]. Two main parameters for such systems are accuracy and measurement range. This parameter space is sketched in Figure 1 for the different measurement principles employed. In terms of accuracy, only schemes based on laser trackers, measuring two angles and one distance, and trilateration or multilateration schemes, measuring at least three distance or distance differences, can potentially compete with the classical coordinate measurement machines (CMM) based on serial kinematics, where a high-precision actuator is used for each degree of freedom. However, while the accuracy of laser trackers is mainly limited by the angular accuracy, multilateration and trilateration schemes can achieve a measurement uncertainty similar to that of the underlying length measurement system, depending on the configuration of the measurement geometry [8].

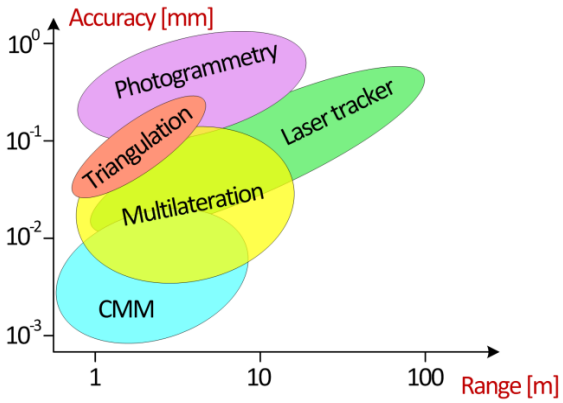

Figure 1. Accuracy and range of classical mechanical coordinate measurement machines (CMM) in comparison to different optical measurement principles, adapted from [3].

While many of the works on multilateration employ single-wavelength heterodyne laser interferometers with sub-µm distance measurement uncertainties [9, 10, 12, 13], the practical applicability of this approach is limited. The interferometric distance measurement has to be incremental, and no absolute distances can be measured. This forbids any interception of the line-of-sight to the retro-reflector target. A measurement principle capable of measuring absolute distances is of key importance for applications in an industrial environment. In this context, optical frequency combs as a metrological tool for precise and absolute distance measurements have received a lot of attention in the last years [14–20]. However, these works concentrate on distance measurements, and no 3D position measurements have been demonstrated so far.

In this paper, we demonstrate 3D position measurements based on trilateration using optical frequency combs. The distances to the retroreflector are absolutely measured using the 240th and 241th harmonic inter-mode beats of the frequency comb formed by a femtosecond pulsed laser with 100 MHz repetition rate. Comparing length measurement results of our system to those obtained from a commercial interferometer, we achieve a length measurement accuracy of 2.2 µm with an integration time of 10 ms. For the used triangular arrangement of three measurement modules spaced by 200 mm this results in a volumetric accuracy of 24 µm. Target tracking is based on MEMS mirrors and four-quadrant diodes. Furthermore we present developments towards a high-sensitivity surface topography sensor employing modulator-based frequency combs with the potential for photonic integration. We demonstrate distance measurements to natural scattering surfaces with acquisition times of 8.3 µs and accuracies better than 10 µm. These data are maintained over a dynamic range of more than 37 dB. Modulator-based frequency comb sources are well suited for photonic integration, which is demonstrated using the silicon-organic hybrid (SOH) integration platform.

2. Distance measurement with inter-mode beats of a frequency comb

The distance measurement scheme employed here is based on the phase evaluation of inter-mode beats of a frequency comb, as first published by Kaoru Minoshima in 2000 [18]. Direct detection of light from a mode-locked laser (MLL) with a high-bandwidth photodiode leads to an electrical signal comprising a multitude of harmonic beat frequencies at integer multiples of the repetition rate. The stability and accuracy of these higher-order harmonics is directly linked to the pulse repetition rate, which can be measured and compared to a frequency standard. Thus, the broad spectrum of a femtosecond pulse laser offers a convenient access to accurate high-frequency signals.

In this work we use a MLL with a repetition rate of 100 MHz and a 3 dB bandwidth of 10 nm centered at a wavelength of 1556 nm. The experimental setup is depicted in Figure 2. Light from the MLL is split using a fiber coupler. One part is incident on a reference photodiode (PD) with a bandwidth of 40 GHz, the other part is directed to a free-space path towards a retroreflector. The reflected light is guided via a circulator to a measurement PD with identical specifications as the reference PD. A heterodyne scheme with two intermediate frequency stages is used to evaluate the

phases of the 240th and 241th harmonic at 24 GHz and 24.1 GHz simultaneously. After pre-amplification and bandpass filtering, the lines of interest are mixed with a 24.04 GHz local oscillator (LO), which is phase-locked to the repetition rate of the MLL. This generates the first intermediate frequencies at 40 MHz and 60 MHz, which maintain the phase relations of the original signals. To evaluate the phases of both lines in reference and measurement paths, the signals are split and the individual lines are filtered by additional bandpass filters, which suppress the corresponding unwanted frequency. Additional LO with frequencies of 39.875 MHz and 39.9 MHz mix the signals to second intermediate frequencies at 100 kHz and 125 kHz. These signals are then analog-to-digital converted, and the phase differences are evaluated in the digital domain.

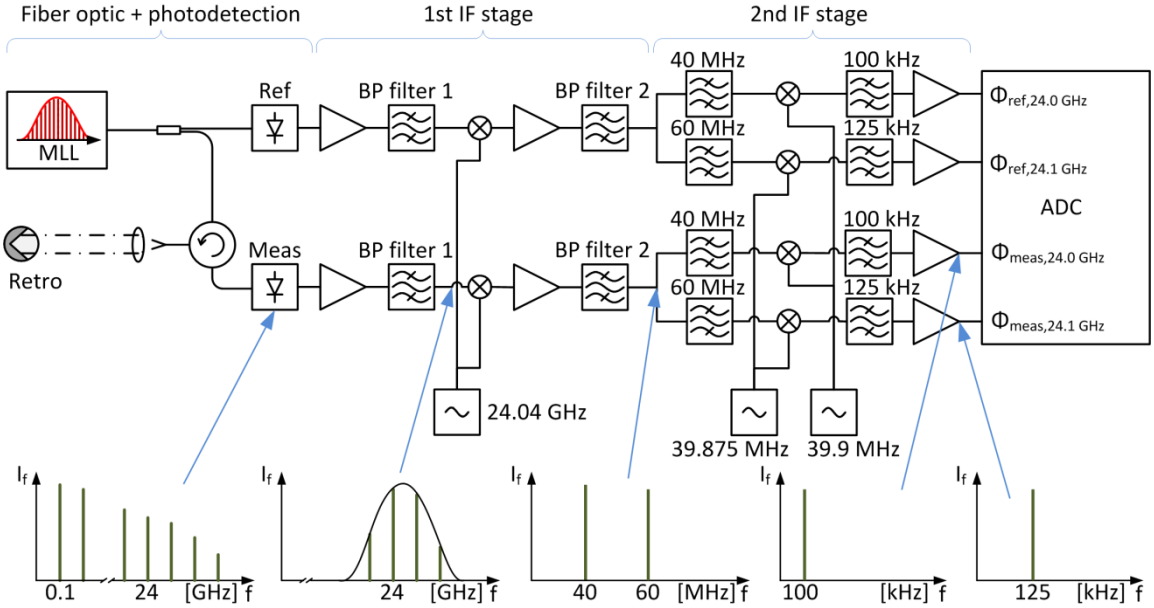

Figure 2. Schematic overview of distance measurement unit and electrical signal spectra (below). Light from a mode-locked laser (MLL) is split in a fiber coupler. One part is detected directly by a reference photodiode (Ref), the other part propagates to the retroreflector (Retro) before it is incident on a measurement photodiode (Meas). The generated electrical beat signals at multiples of the MLL repetition rate are amplified, the 240th and 241th harmonics are band-pass filtered and mixed to first intermediate frequencies of 40 MHz and 60 MHz with a local oscillator (LO) at 24.04 GHz. Further band-pass filters isolate each line, before second intermediate frequencies at 100 kHz and 125 kHz are generated by mixing with a second LO. These signals are analog-to-digital converted (ADC), and the phase differences of reference and measurement signals are evaluated in the digital domain.

The phases $\varphi_{240\text{th}}$ and $\varphi_{241\text{st}}$ of the signals at $f_{240\text{th}} = 24.0\text{GHz}$ and $f_{241\text{st}} = 24.1\text{GHz}$ are measured relative to the reference signal. The optical path length difference $2D$ can be directly calculated from these phases, although the 2π periodicity of the phase limits the unambiguity range of the measurement:

$$\varphi_{240\text{th}} = \left(2\pi \frac{2Df_{240\text{th}}}{c}\right) \bmod 2\pi = \left(2\pi \frac{2D}{\lambda_{240\text{th}}}\right) \bmod 2\pi \tag{1.1}$$

The free-space wavelength of the evaluated beat signal is $\lambda_{240\text{th}} = 12.5\text{mm}$. To extend the absolute measurement range of this fine-scale measurement, the phase difference $\varphi_{241\text{st}} - \varphi_{240\text{th}}$ is evaluated as well:

$$\varphi_{241\text{st}} - \varphi_{240\text{th}} = \left(2\pi \frac{2D\left(f_{241\text{st}} - f_{240\text{th}}\right)}{c}\right) \bmod 2\pi = \left(2\pi \frac{2D}{\Lambda}\right) \bmod 2\pi \tag{1.2}$$

This large-scale measurement with a wavelength $\Lambda = \frac{c}{f_{241th} - f_{240th}} = 3\text{m}$ extends the absolute measurement range significantly. An absolute distance measurement can be made even if the line-of-sight to the retroreflector has been intercepted temporarily.

The measurement results can be seen in Figure 3. The repeatability of the measurement and the influence of the measurement rate were evaluated by repeatedly measuring the distance to a fixed target for different integration times per measurement. The standard deviation is as low as 0.5 µm for an integration time of 50 ms, and fast measurements with update rates of 10 kHz are possible while standard deviations remain in the single-µm regime. The absolute accuracy of the distance measurement was evaluated by comparing to a commercial heterodyne laser interferometer with a specified resolution of 20 pm (Sios MI 5000). The target was incrementally moved along a line with a length of 1 m while recording the relative displacement with the interferometer and simultaneously measuring the distance with our system. The difference in measurement values is plotted in Figure 3(b). The standard deviation of the measurement differences amounts to 2.2 µm. We attribute the observed systematic deviations to residual phase nonlinearities.

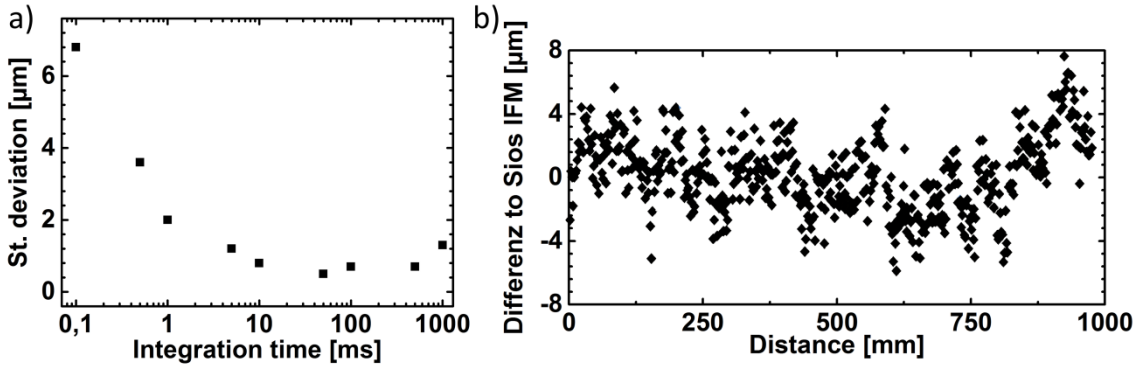

Figure 3. a) Standard deviation of repeated distance measurements to a fixed target as a function of integration time. For integration times of 50 ms, the standard deviation is as low as 0.5 µm. b) Differences of measurement results with 10 ms integration time compared to a commercial HeNe laser interferometer (Sios IFM) for a distance of up to 1 m. The standard deviation of the measurement differences amounts to 2.2 µm.

The optical part of the distance measurement setup relies mainly on comparatively cheap telecommunication-grade fiber-optic components. With the use of fiber couplers and splitters, the light of the single MLL with an optical power of 16 dBm can be easily distributed to three identical receiver units. Combined with MEMS-based tracking optics, this opens the way to measure the 3D-position of a retroreflector by measuring three distances in a trilateration-based approach.

3. µGPS position measurement by trilateration

Many approaches for 3D localization reported in literature use a minimum of four stations and relative distance measurements, e.g. by using single-wavelength interferometry. The redundant number of stations enables a self-calibration with respect to the relative spatial relationship of the stations [9–11]. Such a configuration also allows to determine the initial offset distance to the retroreflector, which is especially important for schemes employing relative distance measurements. However, an interception of the line-of-sight requires a recalibration to again determine the current offset distances to the retroreflector, which have to be added to the measured relative distances. In contrast to these works, we employ a trilateration scheme using only three absolute distance measurements. Our system is calibrated using a similar algorithm as employed in the Global Positioning System (GPS), measuring the distances to a number of known retroreflector positions [21].

Our system comprises only three distance measurement modules with the capability of tracking a retroreflector which are combined in a triangular configuration as depicted in Figure 4(b). The spacing of the modules was chosen to be 200°mm along the sides of the triangle to realize a relatively compact measurement unit. Larger module spacing would result in higher measurement precision at the cost of

a bulkier experimental setup. To calibrate the distance measurement offsets $l_{0,j}$ as well as the relative coordinates (x_j, y_j, z_j) of the pivot points of each module *j*, the distances $d_{i,j}$ to a number *i* of retroreflector positions with known coordinates (x_i, y_i, z_i) are measured for each module. To obtain a good precision, in practice at least 10 different known retroreflector positions are used to obtain pivot point coordinates and the distance measurement offsets. This corresponds to a least-square solution of an over-determined set of equation The wanted parameters are obtained by a minimization:

$$S_j = \sum_i \left| \sqrt{(x_i - x_j)^2 + (y_i - y_j)^2 + (z_i - z_j)^2} + l_{0,j} - d_{i,j} \right|^2$$
$$S_j \to \min \tag{1.3}$$

Experimentally, this is realized by attaching the reflector to a high-precision CMM (Zeiss Eclipse). Once the system is calibrated, three distance measurements are enough to determine the 3D coordinates of the retroreflector, as a possible second solution can be omitted by the known physical layout of the system configuration [22,23].

The tracking of a retroreflecting target while it is moved through space was realized with a MEMS mirror and a four-quadrant (4Q) photodiode. The optical setup is sketched in Figure 4(a). The beam from the fiber collimator is steered by a MEMS-actuated mirror with a mechanical angular range of ±5.5°. To realize a larger tracking volume, angle enlargement optics are used to realize an optical beam deflection of ±30° around a pivot point. The target-tracking feedback loop processes the output of a 4Q photodiode, which is illuminated by using a beam splitter in the optical path.

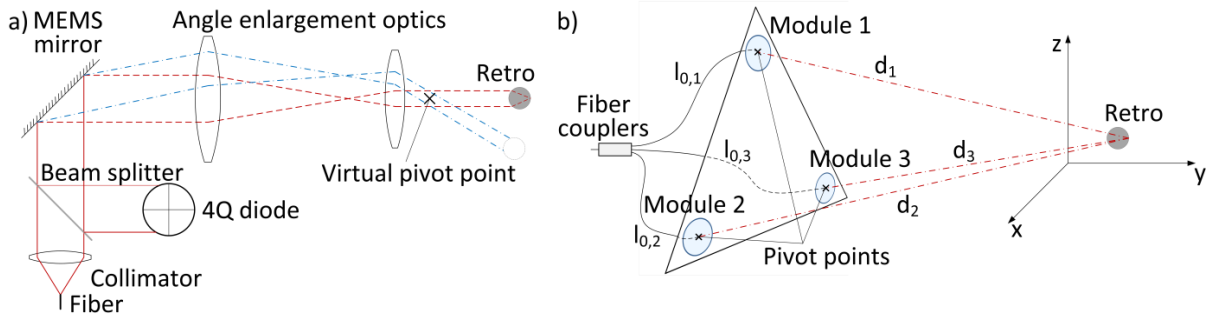

Figure 4. a) Schematic of optical setup for one module. The target is tracked with a four-quadrant photodiode (4Q) and a MEMS mirror. To realize a scanning range of ±30°, optical elements enhance the ±5.5° angle of the MEMS mirror. The beam is mainly deflected around a single pivot point. b) Schematic overview of the GPS-like coordinate measurement. Three fully functional distance measurement modules are arranged in a triangular geometry. They are fed by the same laser source and track a single retroreflector. Coordinate measurements are possible after a calibration, determining the relative coordinates of pivot points and distance offsets $l_{0,i}$, given by the length of the fibers that connect each of the modules.

To characterize the system's accuracy, the same high-precision CMM used for calibration is used to position the target at different locations within a field of 350 × 450 mm^2 roughly 1 m away from the modules. The 3D coordinates are calculated based on the three measured distances d_j acquired with 10 ms integration time. The results are shown in Figure 5. The deviations of the measured coordinates to the set coordinates are plotted as a histogram for X,Y and Z. The measurement geometry and the definition of the axes are the same as defined in Figure 4(b). It is not unexpected that the deviation along the Y axis is the smallest with a standard deviation of 4.4 µm, as the compact module configuration leads to a geometry tending to collinearity for the measurement volume. The measurement standard deviation along X and Z axes amounts to 16…17 µm, leading to a volumetric accuracy of $\sqrt{(16.1\mu m)^2 + (4.4\mu m)^2 + (17.5\mu m)^2} = 24.1\mu m$. These values fit well to a simulation of the measurement geometry with an estimated distance measurement error of 2.2 µm. The simulation leads to a standard deviation in Y direction of 3.4 µm and to standard deviations of 15.0 µm in X, Z

directions. If different geometrical configurations are used, e.g., by placing the modules farther apart, also better accuracies can be achieved [8].

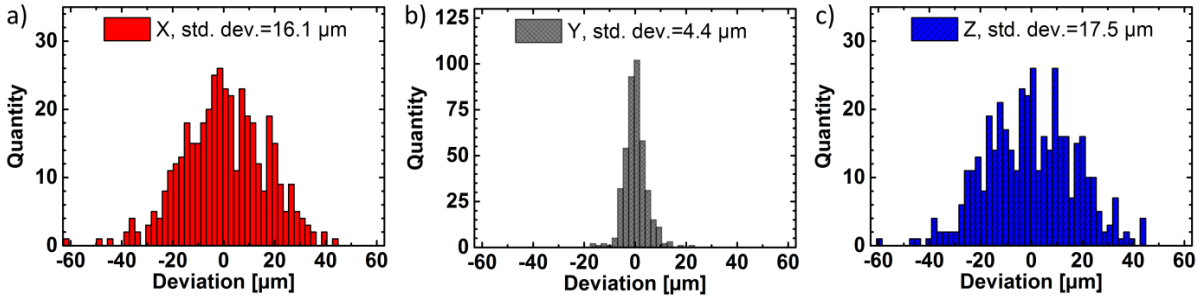

Figure 5. Deviations of optically measured coordinates to set coordinates of a CMM. The measurement geometry and the coordinate axes correspond to those depicted in Figure 4. Values along Y exhibit a smaller variance with a standard deviation of 4.4 µm, while standard deviations along X and Z amount to ~17 µm, resulting in a volumetric error of 24 µm, close to expected values for the chosen configuration with a 200 mm spacing between modules.

4. Modulator-based frequency combs for multi-heterodyne surface topography measurements

Frequency combs generated by mode-locked femtosecond lasers (MLL) typically provide a broadband spectrum with bandwidths of tens of nanometers. Combined with direct detection of the inter-mode beat signals as demonstrated in the sections above, accurate absolute distance measurements are possible. At the expense of increased complexity in the optical domain, the high-frequency electronics for photodetection and phase evaluation can be replaced by slower components with bandwidths of only hundreds of MHz, by employing a second MLL with slightly different line spacing for multi-heterodyne detection [14]. However, considerable technical effort is required to ensure stable drift-free operation of two femtosecond lasers in an industrial environment.

Here we demonstrate distance measurements using continuous-wave (cw) lasers and electro-optic modulators for generation of two frequency combs [24]. In this scheme, the line spacing of the frequency combs is determined by the frequency of the electrical drive signals, which can be precisely adjusted by highly stable RF synthesizers. In contrast to schemes generating only two modulation sidebands for synthetic wavelength interferometry or frequency sweeping methods [25, 26], we generate spectrally flat frequency combs that comprise a multitude of lines with equidistant 40 GHz spacing. The sensitivity of the presented distance measurement method is investigated for different levels of return loss: For optimum return power levels of −13 dBm, we obtain measurement errors of less than 3 µm in an acquisition time of only 8.3 µs, and a measurement error of less than 10 µm can be maintained over a dynamic range of more than 37 dB. The high dynamic range allows a proof-of-principle demonstration of the measurement scheme as a sensitive and fast surface topography sensor. The height of a step in a metal surface is measured and the results are compared to a tactile measurement.

Modulator-based frequency comb sources lend themselves to optical integration, thereby increasing robustness while decreasing size and cost. We demonstrate the realization of nanophotonic frequency comb sources using silicon-organic hybrid (SOH) integration [27]. These sources can be co-integrated with other optical elements available on the silicon-on-insulator SOI platform such as waveguides, splitters and photodiodes, thereby forming a miniaturized distance sensor with a footprint in the mm²-range.

4.1. Experimental setup and measurement principle

The experimental setup of our modulator-based distance measurement system is shown in Figure 6. A pair of Mach-Zehnder modulators (MZM) with carefully adjusted sinusoidal drive signals is used to generate two flat-top frequency combs [28] featuring 7 lines within a power range of 1.25 dB (9 lines within 5.45 dB), see Insets 1 and 2 of Figure 6. The line spacings of the two combs differ by 50 MHz, leading to discrete beat notes when the optical signals are superimposed on a balanced detector (BD) for multi-heterodyne detection, see Inset 3 of Figure 6. To extract the phases of the individual beat

notes, both detector signals are analogue-to-digital converted (A/D, sample rate 3.6 GS/s) and a fast Fourier transform is performed. A portion of the first frequency comb is coupled into the free-space measurement arm, and interferes with a portion of the second comb on BD 1. The phases Φ_m of the detected beat notes are directly linked to the phase shifts that the optical waves accumulate along the measurement arm. As a reference, a second balanced detector (BD 2) is used to detect the beat note phases Ψ_m of the frequency combs before propagation through the measurement arm. After calibration of the initial phases, the phase differences $\Delta\varphi_m = \Phi_m - \Psi_m$ are given by $\Delta\varphi_m = (2\Delta L m\omega_r / c + \Delta\varphi_{0,\Delta L}) \bmod 2\pi$, where $2\Delta L$ is the optical path length difference, ω_r is the line spacing of the comb propagating the measurement arm and $\Delta\varphi_{0,\Delta L}$ is a constant phase offset. After unwrapping the phases obtained from the various beat notes, ΔL can be obtained by a linear fit of $\Delta\varphi_m$ as a function of m. This corresponds to a synthetic wavelength interferometry with a redundant number of wavelengths, making the scheme robust against fluctuations of the measurement signal. No knowledge of the absolute optical wavelengths is needed, as the synthetic wavelengths are solely defined by the spacing ω_r of the measurement comb lines, which is given with very high precision by the RF source used to drive the modulators. The largest synthetic wavelength is linked to the line spacing ω_r of the measurement comb and amounts to $\Lambda = 7.5$ mm, which leads to a range of non-ambiguity of $\Lambda/2 = 3.75$ mm. The measurement path is equipped with a lens system, leading to a Gaussian beam with a waist radius of $w_0 = 13$ µm and a confocal parameter of $b = 340$ µm on the sample side. Less than –8 dBm of output power at around 1550 nm are emitted towards the sample.

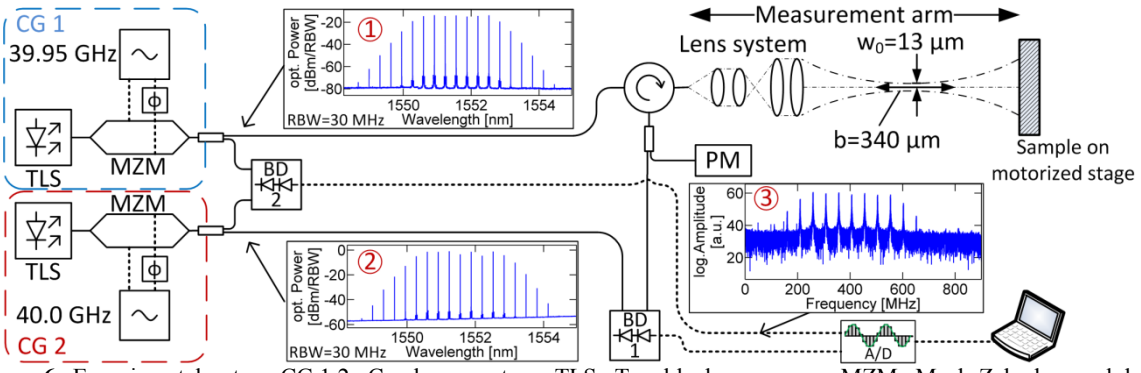

Figure 6. Experimental setup. CG 1,2: Comb generators, TLS: Tunable laser source, MZM: Mach-Zehnder modulator, BD 1,2: Balanced detectors, PM: Power meter, A/D: Analog-to-digital converter; Dashed lines: Electrical connections, Solid lines: Optical fiber. Inset 1+2: Optical spectrum. Inset 3: Electrical spectrum

4.2. Experimental demonstration

To characterize the system, we measure the distance to a plane mirror on a motorized linear translation stage that features a linear encoder with 0.1 µm resolution. The use of the lens system leads to strongly varying power levels at BD 1 when the mirror is moved through its focus. This effect is used to characterize the sensitivity of the system. For measurements of natural scattering surfaces, the sample is kept in focus and the lens system captures scattered light. Each measurement is based on recorded photodiode signals with a duration of 8.3 µs, and the measurement is repeated ten times for each stage position. Figure 7(a) shows the measured distance as a function of stage position along with the corresponding measurement errors; Figure 7(b) shows the power levels along with the standard deviations that were calculated from the ten measurement results obtained at each position. As expected, measurement errors increase for decreasing power levels. Nevertheless, we find that the absolute errors remain smaller than 10 µm over virtually the full range with standard deviations below 4 µm, even though the returned optical power drops by more than 37 dB. Oscillations in the error are attributed to thermal fluctuations in the optical fibers during the experiments, which influence the

optical path lengths. For optimum power levels between -13 dBm and −24 dBm, the error is smaller than 3 µm and sub-µm standard deviations are achieved.

To confirm the viability of the technique when used with naturally scattering surfaces, we measure a step milled into a steel surface, Fig. 2(c). Using a tactile coordinate measurement machine (Carl Zeiss O-Inspect 442), a step height of 464.4 µm was obtained. This is in excellent agreement with the height of 461.2 µm as measured with our system, given the roughness of the steel surface and the limited uniformity of the milled step.

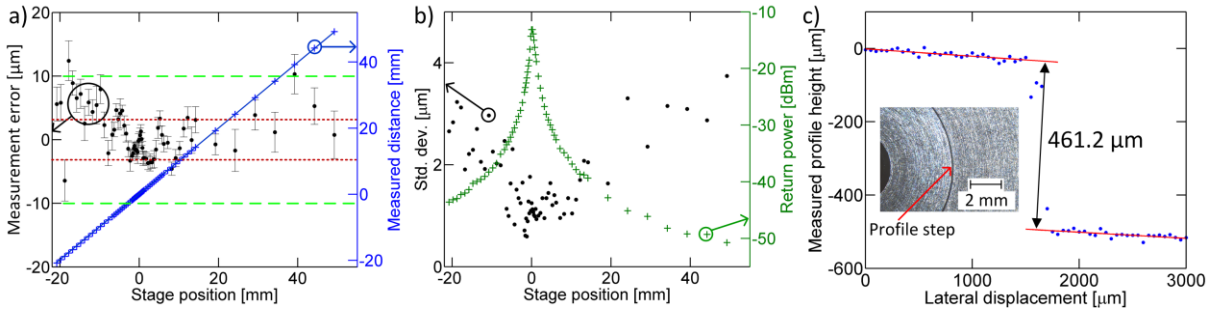

Figure 7. Measurement results obtained with our modulator-based setup. a) Measured distances and errors vs. stage position. Error bars denote the standard deviation from the mean for 10 subsequent measurements taken at each position. Red dotted line marks an error of ±3 µm, green dashed line marks an error of ±10 µm. b) Power coupled back to the measurement detector as a function of stage position along with the standard deviation of 10 subsequent measurements at each stage position (black). c) Measured values for a step milled into a steel surface. The step height as measured with our setup deviates by 3.2 µm from a tactile reference measurement. Inset: Microscopic picture of the surface. The step is indicated by an arrow.

5. Towards an integration on the silicon photonic platform

Silicon photonics offers tremendous potential for large-scale photonic-electronic integration through joint processing of photonic and electronic circuitry and by fabless fabrication. The silicon photonics platform offers a broad portfolio of optical components such as waveguides, phase shifters, splitters and photodetectors [29]. However, to realize a miniaturized distance sensor system on a chip following the principles discussed in the preceding section, it is necessary to realize miniaturized frequency comb sources on the silicon chip. This is a challenging task: The generation of broadband frequency combs requires a large modulation depth to achieve a large number of sidebands along with a high modulation frequency to obtain useful line spacings of tens of gigahertz. This is hard to achieve using conventional silicon photonic phase modulators that exploit free-carrier depletion or injection in p-n, p-i-n, or metal-oxide-semiconductor (MOS) structures [30]. To overcome the limitations of all-silicon devices, we use the concept of silicon-organic hybrid (SOH) integration [31, 32] which combines nanophotonic SOI waveguides with organic cladding materials to realize highly efficient broadband phase shifters [33, 34]. This hybrid integration leads to devices that exhibit voltage-length products down to $U_\pi L = 0.5$ V mm at DC, which allows high modulation depths at low voltages [35]. Using a dual-drive SOH Mach-Zehnder modulator (MZM), we demonstrate generation of a flat-top frequency comb comprising 7 lines with a spacing of 40 GHz and a spectral flatness of 2 dB that are perfectly suited for high-speed data transmission [27].

The SOH phase modulator [33, 35, 36] consists of an optical slot waveguide [37] electrically connected to metallic transmission lines through 60 nm thick doped silicon strips. A schematic cross section and a simulated mode profile of the optical slot waveguide are depicted in Figure 8(a). The modulation voltage applied to the transmission lines drops across the narrow slot, which has a typical width of 100 … 150 nm. This results in a high electric field that strongly overlaps with the optical mode, and this strong overlap leads to highly efficient electro-optic interaction and hence to a low voltage-length product $U_\pi L$. The silicon waveguides are fabricated on a SOI wafer with a 2 µm thick buried oxide and a 220 nm thick device layer using 193 nm deep-UV lithography. After processing the slot waveguides and the transmission lines, the structures are covered with the electro-optic

chromophore DLD164 [35], which entirely fills the slot. The electro-optic cladding is applied by spin coating and poled at elevated temperatures with a DC voltage across the slotline electrodes. More details about the phase modulator can be found in [36]. Our comb generators consist of two phase modulators in a Mach-Zehnder interferometer. These phase modulators are driven independently in a dual-drive configuration and have a length of about 2 mm.

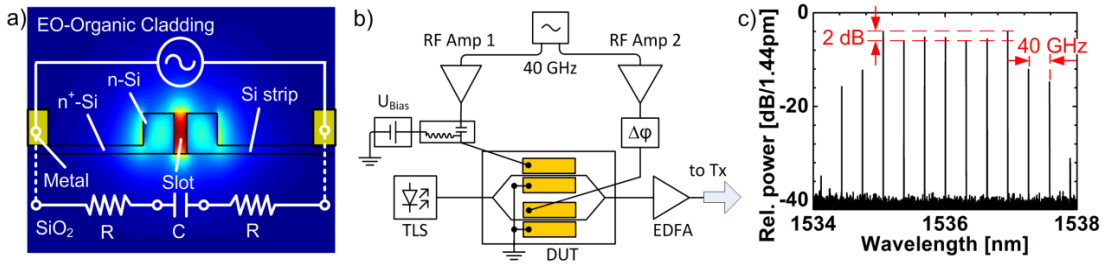

Figure 8. Dual-drive frequency comb generator and corresponding optical spectrum. (a) Schematic cross-section and simulated optical mode of a silicon-organic hybrid (SOH) slot-waveguide phase modulator. The two rails of the silicon slot waveguide are electrically connected to metal electrodes by 60 nm high n-doped silicon strips. The waveguide is covered by an electro-optic cladding material (DLD164), which entirely fills the slot. (b) Integrated dual-drive frequency comb generator: A tunable laser source (TLS) is coupled to a dual-drive SOH Mach-Zehnder modulator (MZM) via grating couplers. The arms are driven by two sinusoidal 40 GHz signals. Flat combs are obtained by carefully adjusting the signal powers and phases along with the bias voltage U_{Bias}. Fiber-chip coupling losses are compensated by an erbium-doped fiber amplifier (EDFA). (c) Flat-top spectrum obtained for electrical drive powers of 28 dBm and 23 dBm measured at the output of the amplifiers, showing 7 lines within 2 dB flatness. The lines are spaced by 40 GHz.

The experimental setup for characterizing the frequency combs is shown in Figure 8(b). A tunable laser source (TLS) is coupled to the chip via grating couplers [38], and the electrodes for the sinusoidal drive signals are contacted with RF probes. Using sinusoidal drive signals with carefully adjusted amplitudes and phases [28], a spectrally flat frequency comb can be generated. The voltage-length product of each phase modulator was measured at DC to be $U_\pi L = 2$ V mm. This allows an efficient generation of higher-order optical sidebands with electrical drive powers of approximately 28 dBm and 23 dBm in the interferometer arms. The resulting optical spectrum is shown in Figure 8(c). We achieve a spectral flatness of 7 lines within 2 dB for spacings 40 GHz. By comparing the measured optical spectrum to simulations, we estimate a peak-to-peak modulation depth in the two MZM arms of 3.6π and 2.7π, respectively. The estimated phase difference of about π matches nicely to theoretical predictions for achieving an optimal flat comb [28].

6. Conclusion

We demonstrate the use of frequency combs for trilateration-based 3D position measurements, and for sensitive surface topography measurements. A frequency comb generated by a MLL is used in combination with direct detection and electrical heterodyne down-mixing to measure the distances from three MEMS-based tracking units to a retroreflector target. The measurements allow a position determination of the target within a measurement time of 10 ms, and a volumetric accuracy of 24 µm using a compact triangular configuration of the measurement modules with 20 cm side length. In a second set of experiments, modulator-based frequency combs are generated from cw lasers and are used with a sensitive multi-heterodyne detection technique for measuring distances to natural scattering surfaces. Measurement errors are below 10 µm over a dynamic range of more than 37 dB. For optimum power levels and integration times of 8.3 µs, the absolute errors become smaller than 3 µm. The comb-generation principle lends itself to photonic integration, and frequency comb sources based on silicon-organic hybrid (SOH) electro-optic modulators are shown.

References

[1] Bridges B, 2012 Technology white paper: Laser Tracker. Available at https://faro.blob.core.windows.net/sitefinity/white-papers/04ref707-012-de---whitepaper_laser-tracker.pdf?sfvrsn=6, accessed on 03.09.2014
[2] Leica Geosystems 2012 Leica absolute interferometer. Available at http://metrology.leica-geosystems.com/downloads123/m1/metrology/general/white-tech-paper/Leica Absolute Interferometer_white paper_en.pdf, accessed on 03.09.2014
[3] Cuypers W, Van Gestel N, Voet A, Kruth J-P, Mingneau J and Bleys P 2009 *Optics and Lasers in Engineering* **47** 292.
[4] Stanley A and Klein M 2010 *Applied Mechanics and Materials* **24-25** 167.
[5] Milanović V, Siu N, Kasturi A, Radojičić M, Su Y, Schenk H and Piyawattanametha W *Proceedings of SPIE* vol. **7930** pp 79300U.
[6] Nikon 2010 K-Series Optical CMM solutions. Available at http://www.nikonmetrology.com/de_EU/content/download/11040/220148/version/4/file/Optical_CMM_EN.pdf, accessed on 03.09.2014
[7] Takatsuji T, Goto M, Kirita A, Kurosawa T and Tanimura Y 2000 *Meas. Sci. Technol.* **11** 477.
[8] Zhang D, Rolt S and Maropoulos P G 2005 *Meas. Sci. Technol.* **16** 2541.
[9] Ibaraki S, Takeuchi K, Yano T, Takatsuji T, Osawa S and Sato O 2011 *Journal of Mechanics Engineering & Automation* **2011** 313.
[10] Schwenke H and Warmann C 2011 10th IMEKO TC14 *Symposium on Laser Metrology for Precision Measurement and Inspection in Industry* Braunschweig, Germany, September 12-14.
[11] Takatsuji T, Goto M, Kurosawa T, Tanimura Y and Koseki Y 1998 *Meas. Sci. Technol.* **9** 38.
[12] Santolaria J, Majarena A C, Samper D, Brau A and Velázquez J 2014 *The Scientific World Journal* **2014** 1.
[13] Linares J-M, Chaves-Jacob J, Schwenke H, Longstaff A, Fletcher S, Flore J, Uhlmann E and Wintering J 2014 *Precision Engineering* **38** 578.
[14] Coddington I, Swann W C, Nenadovic L and Newbury N R 2009 *Nature Photonics* **3** 351.
[15] Cui M, Zeitouny M G, Bhattacharya N, van den Berg S A and Urbach H P 2011 *Opt. Express* **19** 6549.
[16] Hyun S, Kim Y-J, Kim Y, Jin J and Kim S-W 2009 *Meas. Sci. Technol.* **20** 95302.
[17] Kajima M and Minoshima K 2010 *Appl. Opt.* **49** 5844.
[18] Minoshima K and Matsumoto H 2000 *Appl. Opt.* **39** 5512-5517.
[19] Liu T-A, Newbury N R and Coddington I 2011 *Opt. Express* **19** 18501.
[20] Doloca N R, Meiners-Hagen K, Wedde M, Pollinger F and Abou-Zeid A 2010 *Measurement Science and Technology* **21** 115302.
[21] Bancroft S 1985 IEEE Trans. Aerosp. *Electron. Syst.* **21** 56.
[22] Lee J-K, Kim Y, Lee J-H and Kim S-C 2014 IEEE *Commun. Lett.* **18** 1591–1594.
[23] Zhuang H, Li B, Zvi S. Roth and Xie X 1992 *Robotics and Autonomous Systems* **9** 255.
[24] Weimann C, Meier D, Wolf S, Schleitzer Y, Totzeck M, Heinrich A, Hoeller F, Leuthold J, Freude W and Koos C 2013 *Conference on Lasers and Electro-Optics* pp CTu2I.3.
[25] Lay O P, Dubovitsky S, Peters R D, Burger J P, Ahn S-W, Steier W H, Fetterman H R and Chang Y 2003 *Opt. Lett.* **28** 890.
[26] Samuel Choi, Mitsufumi Yamamoto, Daisuke Moteki, Tatsutoshi Shioda, Yosuke Tanaka and Takashi Kurokawa 2006 *Opt. Lett.* **31** 1976.
[27] Weimann C, Schindler P C, Palmer R, Wolf S, Bekele D, Korn D, Pfeifle J, Koeber S, Schmogrow R, Alloatti L, Elder D, Yu H, Bogaerts W, Dalton L R, Freude W, Leuthold J and Koos C 2014 *Opt. Express* **22** 3629.
[28] Sakamoto T, Kawanishi T and Izutsu M 2007 *Opt. Lett.* **32** 1515.
[29] Biberman A and Bergman K 2012 *Reports on Progress in Physics* **75** 46402.
[30] Reed G T, Mashanovich G, Gardes F Y and Thomson D J 2010 *Nature Photonics* **4** 518.
[31] Baehr-Jones T W and Hochberg M J 2008 *J. Phys. Chem. C* **112** 8085.

[32] Brosi J-M, Koos C, Andreani L, Waldow M, Leuthold J and Freude W 2008 *Opt. Express* **16** 4177.
[33] Alloatti L, Korn D, Palmer R, Hillerkuss D, Li J, Barklund A, Dinu R, Wieland J, Fournier M, Fedeli J, Yu H, Bogaerts W, Dumon P, Baets R, Koos C, Freude W and Leuthold J 2011 *Opt. Express* **19** 11841.
[34] Koos C, Brosi J, Waldow M, Freude W and Leuthold J 2007 *Proc. European Conf. on Optical Communication,* paper P056
[35] Palmer R, Koeber S, Heni W, Elder D L, Korn D, Yu H, Alloatti L, Koenig S, Schindler P C, Bogaerts W, Pantouvaki M, Lepage G, Verheyen P, van Campenhout J, Absil P, Baets R, Dalton L R, Freude W, Leuthold J and Koos C 2013 *Proc. European Conf. on Optical Communication,* paper We.3.B.3.
[36] Palmer R, Alloatti L, Korn D, Schindler P C, Baier M, Bolten J, Wahlbrink T, Waldow M, Dinu R, Freude W, Koos C and Leuthold J 2013 *Photonics Technology Letters*, IEEE **25** 1226.
[37] Almeida V R, Xu Q, Barrios C A and Lipson M 2004 *Opt. Lett.* **29** 1209.
[38] Taillaert D, van Laere F, Ayre M, Bogaerts W, van Thourhout D, Bienstman P and Baets R 2006 *Jpn. J. Appl. Phys.* **45** 6071.